

# The dynamics of starvation and recovery

<sup>1</sup> Justin D. Yeakel \* †‡§, Christopher P. Kempes †‡, and Sidney Redner †¶‡

<sup>3</sup> \*School of Natural Science, University of California Merced, Merced, CA, †The Santa Fe Institute, Santa Fe, NM, ¶Department of Physics, Boston University, Boston

<sup>4</sup> MA, ‡Contributed equally, and §To whom correspondence should be addressed: jdyeakel@gmail.com

<sup>5</sup> Submitted to Proceedings of the National Academy of Sciences of the United States of America

<sup>6</sup> The eco-evolutionary dynamics of species are fundamentally linked to the energetic constraints of its constituent individuals. <sup>7</sup> Of particular importance are the tradeoffs between reproduction and the dynamics of starvation and recovery in resource-limited environments. To elucidate the consequences of this tradeoff, <sup>10</sup> we introduce a minimal nutritional state-structured model that incorporates two classes of consumer: nutritionally replete consumers that reproduce, and undernourished, non-reproducing consumers that are susceptible to mortality. As a function of <sup>15</sup> the transition rates between these two states that are determined by the abundance of resources, the consumer populations can either undergo cyclic dynamics or reach a steady state. We obtain <sup>18</sup> strong constraints on starvation and recovery rates by deriving allometric scaling relationships between body size and a variety <sup>20</sup> of traits and find that population dynamics subject to these constraints are typically driven to a steady state. Moreover, we find <sup>22</sup> that these rates fall within a ‘refuge’ in parameter space, where <sup>23</sup> the probability of extinction of the consumer population is minimized. Thus we identify a potential mechanism that may both <sup>25</sup> drive and constrain the dynamics of animal populations. Our <sup>26</sup> model provides a natural framework that predicts maximum body <sup>27</sup> size for mammals by determining the relative stability of an otherwise homogeneous population to a mutant population with altered percentage of body fat. For body masses  $< 1.75 \times 10^7$  g, <sup>30</sup> individuals with increased energetic reserves can invade resident <sup>31</sup> populations, and vice versa for body mass  $> 1.75 \times 10^7$  g, thus <sup>32</sup> providing a principled mechanism for a within-lineage driver of <sup>33</sup> Cope’s rule.

<sup>34</sup> foraging | starvation | reproduction

<sup>35</sup> Significance Statement Energetic investment in somatic maintenance and growth vs. reproduction directly impacts the dynamics of <sup>36</sup> populations among species. Here, we construct a Nutritional State- <sup>37</sup> structured Model (NSM) to assess the population-level effects of star- <sup>38</sup> vation and recovery of a consumer population in a resource-limited en- <sup>39</sup>vironment, and use allometric scaling relationships for mammals to es- <sup>40</sup>tablish all timescales and rates. Our model: i. reveals that mammalian <sup>41</sup> energetic rates minimize the probability of stochastic extinction, ii. es- <sup>42</sup>tablishes dynamic bounds on mammalian body size while providing <sup>43</sup> independent theoretical support for the energy equivalence hypothesis, <sup>44</sup> and iii. provides a mechanistic driver for the evolutionary trend towards <sup>45</sup> larger body size known as Cope’s rule.

## 47 Introduction

<sup>48</sup> The behavioral ecology of all organisms is influenced by the en- <sup>49</sup>ergetic state of individuals, which directly influences how they <sup>50</sup>invest reserves in uncertain environments. Such behaviors are <sup>51</sup>generally manifested as tradeoffs between investing in somatic <sup>52</sup>maintenance and growth, or allocating energy towards repro- <sup>53</sup>duction (1–3). The timing of these behaviors responds to se- <sup>54</sup>lective pressure, as the choice of the investment impacts future <sup>55</sup>fitness (4–6). The influence of resource limitation on an or- <sup>56</sup>ganism’s ability to maintain its nutritional stores may lead to <sup>57</sup>repeated delays or shifts in reproduction over the course of an <sup>58</sup>organism’s life.

<sup>59</sup> The balance between (a) somatic growth and maintenance, <sup>60</sup>and (b) reproduction depends on resource availability (7). For <sup>61</sup>example, reindeer invest less in calves born after harsh winters <sup>62</sup>(when the mother’s energetic state is depleted) than in calves <sup>63</sup>born after moderate winters (8). Many bird species invest dif-

<sup>64</sup>ferently in broods during periods of resource scarcity compared <sup>65</sup>to normal periods (9, 10), sometimes delaying or even foregoing <sup>66</sup>reproduction for a breeding season (1, 11, 12). Even fresh- <sup>67</sup>water and marine zooplankton have been observed to avoid <sup>68</sup>reproduction under nutritional stress (13), and those that do <sup>69</sup>reproduce have lower survival rates (2). Organisms may also <sup>70</sup>separate maintenance and growth from reproduction over space <sup>71</sup>and time: many salmonids, birds, and some mammals return to <sup>72</sup>migratory breeding grounds to reproduce after one or multiple <sup>73</sup>seasons in resource-rich environments where they accumulate <sup>74</sup>nutritional reserves (14–16).

<sup>75</sup> Physiology also plays an important role in regulating repro- <sup>76</sup>ductive expenditures during periods of resource limitation. The <sup>77</sup>data collected thus far has shown that diverse mammals (47 <sup>78</sup>species in 10 families) exhibit delayed implantation, whereby <sup>79</sup>females postpone fetal development (blastocyst implantation) <sup>80</sup>until nutritional reserves can be accumulated (17, 18). Many <sup>81</sup>other species (including humans) suffer irregular menstrual cy- <sup>82</sup>cling and higher abortion rates during periods of nutritional <sup>83</sup>stress (19, 20). In the extreme case of unicellular organisms, <sup>84</sup>nutrition is unavoidably linked to reproduction because the nu- <sup>85</sup>tritional state of the cell regulates all aspects of the cell cycle <sup>86</sup>(21). The existence of so many independently evolved mecha- <sup>87</sup>nisms across such a diverse suite of organisms highlights the im- <sup>88</sup>portance and universality of the fundamental tradeoff between <sup>89</sup>somatic and reproductive investment. However the general dy- <sup>90</sup>namic implications of these constraints are unknown.

<sup>91</sup> Though straightforward conceptually, incorporating the en- <sup>92</sup>ergetic dynamics of individuals (22) into a population-level <sup>93</sup>framework (22, 23) presents numerous mathematical obsta- <sup>94</sup>cles (24). An alternative approach involves modeling the <sup>95</sup>macroscale relations that guide somatic versus reproductive <sup>96</sup>investment in a consumer-resource system. For example, <sup>97</sup>macroscale Lotka-Volterra models assume that the growth rate <sup>98</sup>of the consumer population depends on resource density, thus <sup>99</sup>implicitly incorporating the requirement of resource availability <sup>100</sup>for reproduction (25).

<sup>101</sup> In this work, we adopt an alternative approach in which we <sup>102</sup>explicitly account for resource limitation and the subsequent <sup>103</sup>effects of starvation. Namely, only individuals with sufficient <sup>104</sup>energetic reserves can reproduce. Such a constraint leads to <sup>105</sup>reproductive time lags due to some members of the population <sup>106</sup>going hungry and then recovering. Additionally, we incorporate <sup>107</sup>the idea that reproduction is strongly constrained allometrically <sup>108</sup>(3), and is not generally linearly related to resource density. As

## Reserved for Publication Footnotes

<sup>109</sup> we shall show, these constraints influence the ensuing popula-  
<sup>110</sup> tion dynamics in dramatic ways.

## <sup>111</sup> <sup>112</sup> Nutritional state-structured model (NSM)

<sup>113</sup> We begin by defining a minimal Nutritional State-structured  
<sup>114</sup> population Model (NSM), where the consumer population is  
<sup>115</sup> partitioned into two states: (a) an energetically replete (full)  
<sup>116</sup> state  $F$ , where the consumer reproduces at a constant rate  $\lambda$   
<sup>117</sup> and does not die from starvation, and (b) an energetically defi-  
<sup>118</sup> cient (hungry) state  $H$ , where the consumer does not reproduce  
<sup>119</sup> but dies by starvation at rate  $\mu$ . The underlying resource  $R$   
<sup>120</sup> evolves by logistic growth with an intrinsic growth rate  $\alpha$  and  
<sup>121</sup> a carrying capacity  $C$ . The rate at which consumers transition  
<sup>122</sup> between states and consume resources is dependent on their  
<sup>123</sup> overall abundance, the abundance of resources, the efficiency of  
<sup>124</sup> converting resources into metabolism, and how that metabolism  
<sup>125</sup> is partitioned between maintenance and growth purposes. In  
<sup>126</sup> the supplementary information (SI) we provide a fully mechani-  
<sup>127</sup> stic model for each of these dynamics and constants, and show  
<sup>128</sup> that the system produces a simple non-dimensional form which  
<sup>129</sup> we describe below.

<sup>130</sup> Consumers transition from the full state  $F$  to the hungry  
<sup>131</sup> state  $H$  at a rate  $\sigma$ —the starvation rate—and also in propor-  
<sup>132</sup> tion to the absence of resources ( $1 - R$ ). Conversely, consumers  
<sup>133</sup> recover from state  $H$  to state  $F$  at rate  $\xi\rho$  and in proportion to  
<sup>134</sup>  $R$ , where  $\xi$  represents a ratio between maximal resource con-  
<sup>135</sup> sumption and the carrying capacity of the resource. Resources  
<sup>136</sup> are eaten by the hungry consumers at rate  $\rho R + \delta$ , that accounts  
<sup>137</sup> for their somatic growth ( $\rho R$ ) and maintenance ( $\delta$ ). Full con-  
<sup>138</sup> sumers eat resources at a constant rate  $\beta$  that accounts for max-  
<sup>139</sup> imal maintenance and somatic growth (see SI for mechanistic  
<sup>140</sup> derivations of these rates from resource energetics). The NSM  
<sup>141</sup> represents an ecologically motivated fundamental extension of  
<sup>142</sup> the idealized starving random walk model of foraging, which  
<sup>143</sup> focuses on resource depletion, to include reproduction and re-  
<sup>144</sup> source replenishment (26–28), and is a more general formulation  
<sup>145</sup> than previous models incorporating starvation (29).

In the mean-field approximation, in which the consumers and resources are perfectly mixed, their densities evolve according to the rate equations

$$\begin{aligned}\frac{dF}{dt} &= \lambda F + \xi\rho RH - \sigma(1 - R)F, \\ \frac{dH}{dt} &= \sigma(1 - R)F - \xi\rho RH - \mu H, \\ \frac{dR}{dt} &= \alpha(1 - R)R - (\rho R + \delta)H - \beta F\end{aligned}$$

<sup>146</sup> This system of nondimensional equations follows from a set  
<sup>147</sup> of first-principle relationships for resource consumption and  
<sup>148</sup> growth (see SI for a full derivation and the dimensional form).  
<sup>149</sup> Notice that the total consumer density  $F + H$  evolves accord-  
<sup>150</sup> ing to  $\frac{dF}{dt} + \frac{dH}{dt} = \lambda F - \mu H$ . This resembles the equation of  
<sup>151</sup> motion for the predator density in the classic Lotka-Volterra  
<sup>152</sup> model (30), except that the resource density does not appear in  
<sup>153</sup> the growth term. As discussed above, the attributes of repro-  
<sup>154</sup> duction and mortality have been explicitly apportioned to the  
<sup>155</sup> full and hungry consumers, respectively, so that the growth in  
<sup>156</sup> the total density is decoupled from the resource density.

Equation [1] has three fixed points: two trivial fixed points at  $(F^*, H^*, R^*) = (0, 0, 0)$  and  $(0, 0, 1)$ , and one non-trivial,

internal fixed point at

$$\begin{aligned}F^* &= (\sigma - \lambda) \frac{\alpha\lambda\mu^2(\mu + \xi\rho)}{A(\lambda\rho B + \mu\sigma(\beta\mu + \lambda(\delta + \rho)))}, \\ H^* &= (\sigma - \lambda) \frac{\alpha\lambda^2\mu(\mu + \xi\rho)}{A(\lambda\rho B + \mu\sigma(\beta\mu + \lambda(\delta + \rho)))}, \\ R^* &= (\sigma - \lambda) \frac{\mu}{A}.\end{aligned}\quad [2]$$

<sup>157</sup> where  $A = (\lambda\xi\rho + \mu\sigma)$  and  $B = (\beta\mu\xi + \delta\lambda\xi - \lambda\mu)$ . The sta-  
<sup>158</sup> bility of this fixed point is determined by the Jacobian matrix  
<sup>159</sup>  $\mathbf{J}$ , where each matrix element  $J_{ij} = \partial\dot{X}_i/\partial X_j$  when evaluated  
<sup>160</sup> at the internal fixed point, and  $\mathbf{X}$  is the vector  $(F, H, R)$ . The  
<sup>161</sup> parameters in Eq. [1] are such that the real part of the largest  
<sup>162</sup> eigenvalue of  $\mathbf{J}$  is negative, so that the system is stable with  
<sup>163</sup> respect to small perturbations from the fixed point. Because  
<sup>164</sup> this fixed point is unique, it is the global attractor for all pop-  
<sup>165</sup> ulation trajectories for any initial condition where the resource  
<sup>166</sup> and consumer densities are both nonzero.

<sup>167</sup> From Eq. [2], an obvious constraint on the NSM is that  
<sup>168</sup> the reproduction rate  $\lambda$  must be less than the starvation rate  
<sup>169</sup>  $\sigma$ , so that the consumer and resource densities are positive.  
<sup>170</sup> The condition  $\sigma = \lambda$  thus represents a transcritical (TC) bi-  
<sup>171</sup> furcation (31) that demarcates a physical from an unphysical  
<sup>172</sup> regime where all steady-state densities become negative after in-  
<sup>173</sup> tersecting the trivial fixed point  $(F^*, H^*, R^*) = (0, 0, 0)$ . The  
<sup>174</sup> biological implication of the constraint  $\lambda < \sigma$  has a simple  
<sup>175</sup> interpretation—the rate at which a macroscopic organism loses  
<sup>176</sup> mass due to lack of resources is generally much faster than the  
<sup>177</sup> rate of reproduction. As we will discuss below, this inequality  
<sup>178</sup> is a natural consequence of allometric constraints (3) for organ-  
<sup>179</sup> isms within empirically observed body size ranges.

<sup>180</sup> In the physical regime of  $\lambda < \sigma$ , the fixed point [2] may  
<sup>181</sup> either be a stable node or a limit cycle (Fig. 1). In continuous-  
<sup>182</sup> time systems, a limit cycle arises when a pair of complex con-  
<sup>183</sup> jugate eigenvalues crosses the imaginary axis to attain positive  
<sup>184</sup> real parts (32). This Hopf bifurcation is defined by  $\text{Det}(\mathbf{S}) = 0$ ,  
<sup>185</sup> with  $\mathbf{S}$  the Sylvester matrix, which is composed of the coef-  
<sup>186</sup> ficients of the characteristic polynomial of the Jacobian ma-  
<sup>187</sup> trix (33). As the system parameters are tuned to be within the  
<sup>188</sup> stable regime, but close to the Hopf bifurcation, the amplitude  
<sup>189</sup> of the transient cycles becomes large. Given that ecological  
<sup>190</sup> systems are constantly being perturbed (34), the onset of tran-  
<sup>191</sup> sient cycles, even though they decay with time in the mean-field  
<sup>192</sup> description, can increase the extinction risk (35–37).

<sup>193</sup> When the starvation rate  $\sigma \gg \lambda$ , a substantial fraction  
<sup>194</sup> of the consumers are driven to the hungry non-reproducing  
<sup>195</sup> state. Because reproduction is inhibited, there is a low steady-  
<sup>196</sup> state consumer density and a high steady-state resource den-  
<sup>197</sup> sity. However, if  $\sigma/\lambda \rightarrow 1$  from above, the population is  
<sup>198</sup> overloaded with energetically-replete (reproducing) individuals,  
<sup>199</sup> thereby promoting transient oscillations between the consumer  
<sup>200</sup> and resource densities (Fig. 1). If the starvation rate is low  
<sup>201</sup> enough that the Hopf bifurcation is crossed, these oscillations  
<sup>202</sup> become stable over time. This threshold occurs at higher values  
<sup>203</sup> of the starvation rate as the recovery rate  $\rho$  increases, such that  
<sup>204</sup> the range of parameter space giving rise to cyclic dynamics also  
<sup>205</sup> increases with higher recovery rates.

## <sup>206</sup> Role of allometry

<sup>207</sup> While there are no a priori constraints on the parameters in  
<sup>208</sup> the NSM, most organisms correspond to restricted portions of  
<sup>209</sup> the parameter space. Here we use allometric scaling relations  
<sup>210</sup> to constrain the covariation of rates in a principled and biologi-  
<sup>211</sup> cally meaningful manner. Allometric scaling relations highlight  
<sup>212</sup> common constraints and average trends across large ranges in  
<sup>213</sup> body size and species diversity. Many of these relations can be

derived from a small set of assumptions and below we describe an adjusted starting mass of  $m'_0 = \epsilon_\sigma \epsilon_\lambda M$ , in which case our framework to determine the covariation of timescales and rates across the range of mammals for each of the key parameters of our model (cf. ref. 38). We are thereby able to define the regime of dynamics occupied by the entire class of mammals, along with the key differences between the largest and smallest mammals.

Nearly all of the rates described in the NSM are determined by consumer metabolism, which can be used to describe a variety of organismal features (39). The scaling relation between an organism's metabolic rate  $B$  and its body mass  $M$  at reproductive maturity is known to scale as  $B = B_0 M^\eta$  (40), where the scaling exponent  $\eta$  is typically close to 2/3 or 3/4 for metazoans (e.g., ref. 39), and has taxonomic shifts for unicellular species between  $\eta \approx 1$  in eukaryotes and  $\eta \approx 1.76$  in bacteria (3, 41). Several efforts have shown how a partitioning of  $B$  between growth and maintenance purposes can be used to derive a general equation for both the growth trajectories and growth rates of organisms ranging from bacteria to metazoans (3, 42–45). This relation is derived from the simple balance condition (3, 42–45)

$$B_0 m^\eta = E_m \frac{dm}{dt} + B_m m, \quad [3]$$

where  $E_m$  is the energy needed to synthesize a unit of mass,  $B_m$  is the metabolic rate to support an existing unit of mass, and  $m$  is the mass of the organism at any point in its development. This balance has the general solution (3, 46)

$$\left(\frac{m(t)}{M}\right)^{1-\eta} = 1 - \left[1 - \left(\frac{m_0}{M}\right)^{1-\eta}\right] e^{-a(1-\eta)t/M^{1-\eta}}, \quad [4]$$

where, for  $\eta < 1$ ,  $M = (B_0/B_m)^{1/(1-\eta)}$  is the asymptotic mass,  $a = B_0/E_m$ , and  $m_0$  is mass at birth, itself varying allometrically (see SI). We now use this solution to define the timescale for reproduction and recovery from starvation (Fig. 2; see (43) for a detailed presentation of these timescales). The time that it takes to reach a particular mass  $\epsilon M$  is given by the timescale

$$\tau(\epsilon) = \ln \left[ \frac{1 - (m_0/M)^{1-\eta}}{1 - \epsilon^{1-\eta}} \right] \frac{M^{1-\eta}}{a(1-\eta)}, \quad [5]$$

where we will define values of  $\epsilon$  to describe a set of rates within our model. For the time to reproduce,  $t_\lambda = \tau(\epsilon_\lambda)$ , where  $\epsilon_\lambda$  is the fraction of the asymptotic mass where an organism is reproductively mature and should be close to one (typically  $\epsilon_\lambda \approx 0.95$ ; 42). The growth rate is then given by  $\lambda = \ln(v)/t_\lambda$  where  $v$  is the number of offspring produced, and for any constant value of  $\epsilon_\lambda$ , this rate will scale as  $\lambda \propto M^{\eta-1}$  for  $M \gg m_0$  (3, 42–45).

The rate of recovery  $\rho = 1/t_\rho$  requires that an organism accrues sufficient tissue to transition from the hungry to the full state. Since only certain tissues can be digested for energy (for example the brain cannot be degraded to fuel metabolism),

we define the rates for starvation, death, and recovery by the timescales required to reach, or return from, specific fractions

of the replete-state mass (Fig. 3; see SI, Table I for parameterizations). We define  $m_\sigma = \epsilon_\sigma M$ , where  $\epsilon_\sigma < 1$  is the fraction of replete-state mass where reproduction ceases. This fraction will deviate from a constant if tissue composition systematically scales with adult mass. For example, making use of the observation that body fat in mammals scales with overall body size according to  $M_{\text{fat}} = f_0 M^\gamma$  and assuming that once this mass is fully digested the organism starves, this would imply that  $\epsilon_\sigma = 1 - f_0 M^\gamma / M$ . It follows that the recovery timescale,  $t_\rho$ , is the time to go from  $m = \epsilon_\sigma \epsilon_\lambda M$  to  $m = \epsilon_\lambda M$  (Fig. 2). Using Eqs. [4] and [5] this timescale is given by simply considering

$$t_\rho = \ln \left[ \frac{1 - (\epsilon_\sigma \epsilon_\lambda)^{1-\eta}}{1 - \epsilon_\lambda^{1-\eta}} \right] \frac{M^{1-\eta}}{a'(1-\eta)} \quad [6]$$

where  $a' = B_0/E'_m$  accounts for possible deviations in the biosynthetic energetics during recovery (see SI). It should be noted that more complicated ontogenetic models explicitly handle storage (45), whereas this feature is implicitly covered by the body fat scaling in our framework.

To determine the starvation rate,  $\sigma$ , we are interested in the time required for an organism to go from a mature adult that reproduces at rate  $\lambda$ , to a reduced-mass hungry state where reproduction is impossible. For starving individuals we assume that an organism must meet its maintenance requirements by using the digestion of existing mass as the sole energy source. This assumption implies the following simple metabolic balance

$$\frac{dm}{dt} E'_m = -B_m m \quad [7]$$

or

$$\frac{dm}{dt} = -\frac{a'}{M^{1-\eta}} m \quad [8]$$

where  $E'_m$  is the amount of energy stored in a unit of existing body mass, which differs from  $E_m$ , the energy required to synthesize a unit of biomass (45). Given the replete mass,  $M$ , of an organism, the above energy balance prescribes the mass trajectory of a non-consuming organism:

$$m(t) = M e^{-a't/M^{1-\eta}}. \quad [9]$$

The timescale for starvation is given by the time it takes  $m(t)$  to reach  $\epsilon_\sigma M$ , which gives

$$t_\sigma = -\frac{M^{1-\eta}}{a'} \ln(\epsilon_\sigma). \quad [10]$$

The starvation rate is then  $\sigma = 1/t_\sigma$ , which scales with replete-state mass as  $1/M^{1-\eta} \ln(1 - f_0 M^\gamma / M)$ . An important feature is that  $\sigma$  does not have a simple scaling dependence on  $\lambda$  (Fig. 3), which is important for the dynamics that we later discuss.

The time to death should follow a similar relation, but defined by a lower fraction of replete-state mass,  $m_\mu = \epsilon_\mu M$  where  $\epsilon_\mu < \epsilon_\sigma$ . Suppose, for example, that an organism dies once it has digested all fat and muscle tissues, and that muscle tissue scales with body mass according to  $M_{\text{musc}} = u_0 M^\zeta$ . This gives  $\epsilon_\mu = 1 - (f_0 M^\gamma + u_0 M^\zeta) / M$ . Muscle mass has been shown to be roughly proportional to body mass (47) in mammals and thus  $\epsilon_\mu$  is merely  $\epsilon_\sigma$  minus a constant. The time to go from starvation to death is the total time to reach  $\epsilon_\mu M$  minus the time to starve, or

$$t_\mu = -\frac{M^{1-\eta}}{a'} \ln(\epsilon_\mu) - t_\sigma, \quad [11]$$

Although the rate equations [1] are general, here we focus on parameterizations for terrestrial-bound endotherms, specifically mammals, which range from a minimum of  $M \approx 1$  g to a maximum of  $M \approx 10^7$  g (the early Oligocene Indricotheriinae and the Miocene Deinotheriinae). Investigating other classes of organisms would simply involve altering the metabolic exponents and scalings associate with  $\epsilon$ . Moreover, we emphasize that our allometric equations describe mean relationships, and do not account for the variance associated with individual species.

**319 Stabilizing effects of allometric constraints**

320 As the allometric derivations of the NSM rate laws reveal, star-  
321 vation and recovery rates are not independent parameters, and  
322 the biologically relevant portion of the phase space shown in  
323 Fig. 1 is constrained via covarying parameters. Given the pa-  
324 rameters of terrestrial endotherms, we find that the starvation  
325 rate  $\sigma$  and the recovery rate  $\rho$  are constrained to lie within a  
326 small region of potential values (Fig. 4) for the known range  
327 of body sizes  $M$ . We thus find that the dynamics for all mam-  
328 malian body sizes are confined to the steady-state regime of the  
329 NSM and that limit-cycle behavior is precluded. Incorporating  
330 uncertainty in allometric parameters (20% variation around the  
331 mean; Fig. 4), we find that, for larger  $M$ , the distance to the TC  
332 and Hopf bifurcation decreases. These results suggest that small  
333 mammals are marginally less prone to population oscillations—  
334 both stable limit cycles and transient cycles—than mammals  
335 with larger body size. However, starvation and recovery rates  
336 across all values of  $M$  fall squarely in the steady state region at  
337 some distance from the Hopf bifurcation. This result suggests  
338 that cyclic population dynamics should be rare, particularly in  
339 environments where resources are limiting.

340 It should be noted that previous studies used allometric  
341 constraints to explain the periodicity of cyclic populations (48–  
342 50), suggesting a period  $\propto M^{0.25}$ . However this relation seems  
343 to hold only for some species (51), and potential drivers of vari-  
344 ation and systematically different behavior range from predator  
345 and/or prey lifespans to competitive dynamics (52, 53). Statis-  
346 tically significant support for the existence of population cycles  
347 among mammals is relatively rare, though predominantly based  
348 on time series for small mammals (54). However the longer ges-  
349 tational times and increased difficulty in collecting adequate  
350 data precludes obtaining similar-quality information for larger  
351 organisms.

**352 Extinction risk**

353 Within our model, higher rates of starvation result in a larger  
354 flux of the population to the hungry state. In this state, re-  
355 plored. We argue that the NSM provides a suitable framework  
356 to explore these issues.

357 production is absent, thus increasing the likelihood of extinc-  
358 tion. From the perspective of population survival, it is the rate  
359 of starvation relative to the rate of recovery that determines  
360 the long-term dynamics of the various species (Fig. 1). We  
361 therefore examine the competing effects of cyclic dynamics vs.  
362 changes in steady-state density on extinction risk, both as func-  
363 tions of  $\sigma$  and  $\rho$ . To this end, we computed the probability of ex-  
364 tinction, where we define extinction as a population trajectory  
365 falling below one fifth of the allometrically constrained steady  
366 state at any time between  $t = 10^5$  and  $t \leq 10^8$ . This proce-  
367 dure is repeated for 50 replicates of the continuous-time system  
368 shown in Eq. 1 for an organism of  $M = 100$  grams. In each  
369 replicate the initial densities are chosen to be  $(X^*, H^*, R^*)$ ,  
370 with  $X$  a random variable that is uniformly distributed in  $[0, 2]$ .  
371 By allowing the rate of starvation to vary, we assessed extinc-  
372 tion risk across a range of values for  $\sigma$  and  $\rho$  between ca.  $10^{-7}$   
373 to  $10^{-3}$ . As expected, higher rates of extinction correlate with  
374 both high values of  $\sigma$  if  $\rho$  is small, and high values of  $\rho$  if  $\sigma$   
375 is small. For low values of  $\sigma$  and high values of  $\rho$ , the in-  
376 creased extinction risk results from transient cycles with larger  
377 amplitudes as the system nears the Hopf bifurcation (Fig. 5).  
378 For high values of  $\sigma$  and low values of  $\rho$ , increased extinction  
379 risk arises because of the decrease in the steady-state consumer  
380 population density (Figs. 1B, 5). This interplay creates an ‘ex-  
381 tinction refuge’, such that for a constrained range of  $\sigma$  and  $\rho$ ,  
382 extinction probabilities are minimized.

383 We find that the allometrically constrained values of  $\sigma$  and  
384  $\rho$  fall squarely within the extinction refuge (Fig. 5, white point).  
385 These values are close enough to the Hopf bifurcation to avoid  
386 amplitude transient cycles. The feature that allometric values  
387 of  $\sigma$  and  $\rho$  fall within this relatively small window supports  
388 the possibility that a selective mechanism has constrained the  
389 physiological conditions that drive starvation and recovery rates  
390 within populations. Such a mechanism would select for organ-  
391 ism physiology that generates appropriate  $\sigma$  and  $\rho$  values that  
392 serve to minimize extinction risk. This selection could occur  
393 via the tuning of body fat percentages, metabolic rates, and  
394 biomass maintenance efficiencies. *To summarize, our finding*  
395 *that the allometrically-determined parameters fall within this*  
396 *low extinction probability region suggests that the NSM dynam-*  
397 *ics may both drive—and constrain—natural animal populations.*

**398 Dynamic and energetic barriers to body size**

399 Metabolite transport constraints are widely thought to place  
400 strict boundaries on biological scaling (39, 55, 56) and thereby  
401 lead to specific predictions on the minimum possible body size  
402 for organisms (57). Above this bound, a number of energetic  
403 costs and benefits associated with larger body masses, partic-  
404 ularly for mammals. One important such example is the *fast-*  
405 *ing endurance hypothesis*, which contends that larger body size,  
406 with consequent lower metabolic rates and increased ability to  
407 maintain more endogenous energetic reserves, may buffer or-  
408 ganisms against environmental fluctuations in resource avail-  
409 ability (58). Over evolutionary time, terrestrial mammalian lin-  
410 eages show a significant trend towards larger body size (known  
411 as Cope’s rule) (59–62), and it is thought that within-lineage  
412 drivers generate selection towards an optimal upper bound of  
413 roughly  $10^7$  grams (59), a value that is likely limited by higher  
414 extinction risk for large taxa over longer timescales (60). These  
415 trends are thought to be driven by a combination of climate  
416 change and niche availability (62); however the underpinning  
417 energetic costs and benefits of larger body sizes, and how they  
418 influence dynamics over ecological timescales, have not been ex-  
419 plained. We argue that the NSM provides a suitable framework  
420 to explore these issues.

421 The NSM correctly predicts that species with smaller  
422 masses have larger steady-state population densities (Fig. 6A).  
423 Moreover, we show that the NSM provides independent the-  
424 oretical support for the energy equivalence hypothesis and  
425 Damuth’s Law (63–65). The energy equivalence hypothesis ar-  
426 gues that the total energy use,  $B_{\text{tot}}$ , of a population is constant  
427 independent of species size (e.g., (63–65)). This hypothesis is  
428 based on observations showing that the steady state abundance,  
429 metabolism ( $N^* \propto M^{-3/4}/B_0$ ) (e.g., (64, 65)). This relation-  
430 ship implies that  $B_{\text{tot}} = N^*B(M) = Q$ , where  $Q$  is a constant,  
431 and has been shown to hold in both mammalian and vascular  
432 plant communities (63–65). Figure 6A shows that both  $F^*$  and  
433  $H^*$  scale as  $M^{-\eta}$  over a wide range of organism sizes and Fig-  
434 ure 6B shows that  $F^*B$  is nearly constant over this same range.  
435 This result is remarkable because it illustrates that the steady  
436 state values of the NSM combined with the derived timescales  
437 naturally give rise to energy equivalence. Our model shows that  
438 the equivalence breaks down at the maximum observed body  
439 sizes for mammals, suggesting that this maximum is a hard  
440 limit where deviations outside of this range are energetically  
441 suboptimal. In the framework of our model, the total metabolic  
442 rate of  $F$  and  $H$  becomes infinite at a finite mass, and occur at  
443 the same scale where the steady state resources vanish (Fig. 6).  
444 This asymptotic behavior is governed by body sizes at which  
445  $\epsilon_\mu$  and  $\epsilon_\lambda$  equal zero causing the timescales to become infinite  
446 (see Equation 11) and the rates  $\mu$  and  $\lambda$  to equal zero. The  
447  $\mu = 0$  asymptote occurs first when  $f_0 M^{\gamma-1} + u_0 M^{\zeta-1} = 1$ ,  
448 and corresponds to  $(F^*, H^*, R^*) = (0, 0, 0)$ . This point pre-  
449 dicts a strong upper bound on mammalian body size and oc-

453 curs at  $M_{\max} = 6.54 \times 10^7$ . Moreover,  $M_{\max}$ , which is entirely 520 dependent estimates of the largest land mammals, the early 454 determined by the population-level consequences of energetic 521 Oligocene *Indricotherium* at ca.  $1.5 \times 10^7$  g and the late Miocene 455 constraints, is close to the maximum body size observed in the 522 *Deinotherium* at ca.  $1.74 \times 10^7$  g (61). Additionally, our calcula- 456 North American mammalian fossil record (59), as well as the 523 prediction of  $M_{\text{opt}}$  as a function of mass-dependent physiological rates 457 mass predicted from an evolutionary model of body size evolu- 524 is similar to theoretical estimates of maximum body size (60), 458 tion (60). It should be noted that the asymptotic behavior and 525 and provides independent theoretical support for the observa- 459 predicted upper bound depend only on the scaling of body com- 526 tion of a ‘maximum body size attractor’ for North American 460 position and are independent of the resource parameters. We 527 mammals outlined by Alroy (59). While the state of the envi- 461 also note that the prediction of an asymptotic limit on mam- 528 ronment, as well as the competitive landscape, will determine 462 malian size parallels work on microbial life where an upper and 529 whether specific body sizes are selected for or against (62), we 463 lower bound on bacterial size, and an upper bound on single cell 530 propose that the dynamics of starvation and recovery described 464 eukaryotic size, is predicted from similar growth and energetic 531 in the NSM provide a general within-lineage mechanism for the 465 scaling relationships (3, 66).

466 We contend that the NSM provides a mechanistic under- 533 The energetics associated with somatic maintenance, 467 standing of the energetic dynamics that give rise to both ob- 534 growth, and reproduction are important elements that influence 468 served limitations on mammalian body size, as well as the ob- 535 the dynamics of all populations (11). The NSM is a minimal 469 served trend towards larger body size over evolutionary time. 536 and general model that incorporates the dynamics of starvation 470 The NSM predicts that the steady state resource density  $R^*$  537 and recovery that are expected to occur in resource-limited en- 471 decreases with increasing body size of the consumer popula- 538 vironments. By incorporating allometric relations between the 472 tion (Fig. 6C), and classic resource competition theory predicts 539 rates in the NSM, we found: (i) different organismal masses 473 that the species surviving on the lowest resource abundance will 540 have distinct population dynamic regimes, (ii) allometrically- 474 outcompete others (67–69). Thus, the combined NSM steady- 541 determined rates of starvation and recovery appear to minimize 475 state dynamics and allometric timescales predict that larger 542 extinction risk, and (iii) the dynamic consequences of these rates 476 mammals have an intrinsic competitive advantage given a com- 543 may introduce additional drivers and hard boundaries on the 477 mon resource, but does not offer a within-lineage mechanism by 544 evolution of maximum body size. We suggest that the NSM 478 which larger body sizes are selected for. 545 offers a means by which the dynamic consequences of energetic

479 To examine whether the NSM could provide such a mecha- 546 constraints can be assessed using macroscale interactions be- 480 nism, we begin by noting that a theoretical upper bound on 547 tween and among species. Future efforts will involve exploring 481 mammalian body size is given by  $\epsilon_\sigma = 0$ , where mammals 548 the consequences of these dynamics in a spatially explicit frame- 482 are entirely composed of metabolic reserves, and this occurs 549 work, thus incorporating elements such as movement costs and 483 at  $M = 8.3 \times 10^8$ , or 120 times the mass of a male African ele- 550 spatial heterogeneity, which may elucidate additional tradeoffs 484 phant. Next we examine to what extent a more realistic upper 551 associated with the dynamics of starvation and recovery.

485 bound to body mass may serve as an evolutionary attractor, 546 thus providing a suitable within-lineage mechanism for Cope’s 486 rule. We directly assess the susceptibility of an otherwise ho- 487 mogeneouse population to invasion by a mutated subset of the 488 population (denoted by  $'$ ) where individuals have a modified 489 proportion of body fat  $M' = M(1+\chi)$ . For the allowable values 490 of  $\chi$  the adjusted mass should exceed the amount of body fat, 491  $1+\chi > \epsilon_\sigma$ , and the adjusted time to reproduce must be positive, 492 which given Equation 5, implies that  $1 - \epsilon_\lambda^{1-\eta}(1+\chi)^{1-\eta} > 0$ . 493 Together these conditions imply that  $\chi \in (-f_0 M^{\gamma-1}, 1/\epsilon_\lambda - 1)$ , 494 where the upper bound approximately equals 0.05. The modi- 495 fied mass adjusts our model via the altered rates of starvation 496  $\sigma(M')$ , recovery  $\rho(M')$ , and the maintenance of both starving 497  $\delta(M')$  and full consumers  $\beta(M')$ . Importantly,  $\epsilon_\sigma$ , which deter- 498 mines the point along the growth curve that defines the state 499 of starved foragers, is assumed to remain unchanged for the 500 invader population (see SI for detailed derivations of invader 501 rates).

502 To assess the susceptibility of the resident population to 566 invasion, we determine which consumer has a lower steady- 567 state resource density for a given value of  $\chi$ , again with the 568 expectation that populations able to survive on lower resource 569 densities have a competitive advantage (67). We find that for 570  $M \leq 1.75 \times 10^7$  g, having additional body fat ( $\chi > 0$ ) results in 571 lower steady state resource density ( $R'^* < R^*$ ), such that the 572 invader has an intrinsic competitive advantage over the resident 573 population. However, for  $M > 1.75 \times 10^7$  g, leaner individuals 574 ( $\chi < 0$ ) have lower resource steady state densities, switching 575 the advantage for higher values of  $M$ .

576 The observed switch in susceptibility as a function of  $\chi$  at 577  $M_{\text{opt}} = 1.75 \times 10^7$  g thus serves as an attractor, such that the 578 NSM predicts organismal mass to increase if  $M < M_{\text{opt}}$  and 579 decrease if  $M > M_{\text{opt}}$ . This value is close to but smaller than 580 the asymptotic upper bound for terrestrial mammal body size 581 predicted by the NSM, however it is remarkably close to in-

## References

1. Martin TE (1987) Food as a Limit on Breeding Birds: A Life-History Perspective. *Annu. Rev. Ecol. Syst.* 18:453–487.
2. Kirk KL (1997) Life-History Responses to Variable Environments: Starvation and Reproduction in Planktonic Rotifers. *Ecology* 78:434–441.
3. Kempes CP, Dutkiewicz S, Follows MJ (2012) Growth, metabolic partitioning, and the size of microorganisms. *PNAS* 109:495–500.
4. Mangel M, Clark CW (1988) *Dynamic Modeling in Behavioral Ecology* (Princeton University Press, Princeton).
5. Mangel M (2014) Stochastic dynamic programming illuminates the link between environment, physiology, and evolution. *B. Math. Biol.* 77:857–877.
6. Yeakel JD, Dominy NJ, Koch PL, Mangel M (2014) Functional morphology, stable isotopes, and human evolution: a model of consilience. *Evolution* 68:190–203.
7. Morris DW (1987) Optimal Allocation of Parental Investment. *Oikos* 49:332.
8. Tveraa T, Fauchald P, Henaug C, Yoccoz NG (2003) An examination of a compensatory relationship between food limitation and predation in semi-domestic reindeer. *Oecologia* 137:370–376.
9. Daan S, Dijkstra C, Drent R, Meijer T (1988) *Food supply and the annual timing of avian reproduction*.
10. Jacot A, Valeu M, van Oers K, Kempenaers B (2009) Experimental nest site limitation affects reproductive strategies and parental investment in a hole-nesting passerine. *Animal Behaviour* 77:1075–1083.
11. Stearns SC (1989) Trade-Offs in Life-History Evolution. *Funct. Ecol.* 3:259.

- 584 12. Barboza P, Jorde D (2002) Intermittent fasting during win- 651  
 585 ter and spring affects body composition and reproduction 652  
 586 of a migratory duck. *J Comp Physiol B* 172:419–434. 653
- 587 13. Threlkeld ST (1976) Starvation and the size structure of 654  
 588 zooplankton communities. *Freshwater Biol.* 6:489–496. 655
- 589 14. Weber TP, Ens BJ, Houston AI (1998) Optimal avian mi- 656  
 590 gration: A dynamic model of fuel stores and site use. *Evo- 657  
 591 lutionary Ecology* 12:377–401. 658
- 592 15. Mduma SAR, Sinclair ARE, Hilborn R (1999) Food regu- 659  
 593 lates the Serengeti wildebeest: a 40-year record. *J. Anim. 660  
 594 Ecol.* 68:1101–1122. 661
- 595 16. Moore JW, Yeakel JD, Peard D, Lough J, Beere M (2014) 662  
 596 Life-history diversity and its importance to population sta- 663  
 597 bility and persistence of a migratory fish: steelhead in two 664  
 598 large North American watersheds. *J. Anim. Ecol.* 83:1035– 665  
 599 1046. 666
- 600 17. Mead RA (1989) in *Carnivore Behavior, Ecology, and Evo- 667  
 601 lution* (Springer US, Boston, MA), pp 437–464. 668
- 602 18. Sandell M (1990) The Evolution of Seasonal Delayed Im- 669  
 603 plantation. *The Quarterly Review of Biology* 65:23–42. 670
- 604 19. Bulik CM, et al. (1999) Fertility and Reproduction in 671  
 605 Women With Anorexia Nervosa. *J. Clin. Psychiatry* 672  
 606 60:130–135. 673
- 607 20. Trites AW, Donnelly CP (2003) The decline of Steller sea 674  
 608 lions *Eumetopias jubatus* in Alaska: a review of the nutri- 675  
 609 tional stress hypothesis. *Mammal Review* 33:3–28. 676
- 610 21. Glazier DS (2009) Metabolic level and size scaling of rates 677  
 611 of respiration and growth in unicellular organisms. *Funct. 678  
 612 Ecol.* 23:963–968. 679
- 613 22. Kooijman SALM (2000) *Dynamic Energy and Mass Bud- 680  
 614 gets in Biological Systems* (Cambridge). 681
- 615 23. Sousa T, Domingos T, Poggiale JC, Kooijman SALM 682  
 616 (2010) Dynamic energy budget theory restores coherence 683  
 617 in biology. *Philos. T. Roy. Soc. B* 365:3413–3428. 684
- 618 24. Diekmann O, Metz JAJ (2010) How to lift a model for in- 685  
 619 dividual behaviour to the population level? *Philos. T. Roy. 686  
 620 Soc. B* 365:3523–3530. 687
- 621 25. Murdoch WW, Briggs CJ, Nisbet RM (2003) *Consumer- 688  
 622 resource Dynamics*, Monographs in population biology 689  
 623 (Princeton University Press). 690
- 624 26. Benichou O, Redner S (2014) Depletion-Controlled Starva- 691  
 625 tion of a Diffusing Forager. *arXiv*. 692
- 626 27. Bénichou O, Chupeau M, Redner S (2016) Role of Deple- 693  
 627 tion on the Dynamics of a Diffusing Forager. 694
- 628 28. Chupeau M, Bénichou O, Redner S (2016) Universality 695  
 629 classes of foraging with resource renewal. *Phys. Rev. E* 696  
 630 93:032403. 697
- 631 29. Persson L, Leonardsson K, De Roos AM, Gyllenberg M, 698  
 632 Christensen B (1998) Ontogenetic Scaling of Foraging Rates 699  
 633 and the Dynamics of a Size-Structured Consumer-Resource 700  
 634 Model. *Theoretical Population Biology* 54:270–293. 701
- 635 30. Murray JD (2011) *Mathematical Biology: I. An Introduct- 702  
 636 ion*, Interdisciplinary Applied Mathematics (Springer New 703  
 637 York) Vol. 110. 704
- 638 31. Strogatz SH (2008) *Nonlinear Dynamics and Chaos*, With 705  
 639 Applications to Physics, Biology, Chemistry, and Engineer- 706  
 640 ing (Westview Press). 707
- 641 32. Guckenheimer J, Holmes P (1983) *Nonlinear oscilla- 708  
 642 tions, dynamical systems, and bifurcations of vector fields* 709  
 643 (Springer, New York). 710
- 644 33. Gross T, Feudel U (2004) Analytical search for bifurcation 711  
 645 surfaces in parameter space. *Physica D* 195:292–302. 712
- 646 34. Hastings A (2001) Transient dynamics and persistence of 713  
 647 ecological systems. *Ecol. Lett.* 4:215–220. 714
- 648 35. Neubert M, Caswell H (1997) Alternatives to resilience for 715  
 649 measuring the responses of ecological systems to perturba- 716  
 650 tions. *Ecology* 78:653–665. 717
36. Caswell H, Neubert MG (2005) Reactivity and transient 651  
 37. dynamics of discrete-time ecological systems. *Journal of 652  
 38. Difference Equations and Applications* 11:295–310. 653
39. Neubert M, Caswell H (2009) Detecting reactivity. *Ecology*. 654
40. Yodzis P, Innes S (1992) Body Size and Consumer-Resource 655  
 41. Dynamics. *Am. Nat.* 139:1151–1175. 656
42. Brown J, Gillooly J, Allen A, Savage V, West G (2004) Tow- 657  
 43. toward a metabolic theory of ecology. *Ecology* 85:1771–1789. 658
44. DeLong JP, Okie JG, Moses ME, Sibly RM, Brown JH (2010) Shifts in metabolic scaling, production, and efficiency across major evolutionary transitions of life. *PNAS* 107:12941–12945. 659
45. West GB, Brown JH, Enquist BJ (2001) A general model 660  
 46. for ontogenetic growth. *Nature* 413:628–631. 661
47. Moses ME, et al. (2008) Revisiting a Model of Ontogenetic 662  
 48. Growth: Estimating Model Parameters from Theory and 663  
 49. Data. <http://dx.doi.org.proxy.lib.sfu.ca/10.1086/679735> 664  
 171:632–645. 665
50. Gillooly JF, Charnov EL, West GB, Savage VM, Brown JH 666  
 51. (2002) Effects of size and temperature on developmental 667  
 52. time. *Nature* 417:70–73. 668
53. Hou C, et al. (2008) Energy Uptake and Allocation During 669  
 54. Ontogeny. *Science* 322:736–739. 670
55. Bettencourt LMA, Lobo J, Helbing D, Kuhnert C, West 671  
 56. GB (2007) Growth, innovation, scaling, and the pace of life 672  
 57. in cities. *Proc. Natl. Acad. Sci. USA* 104:7301–7306. 673
58. Folland JP, Mc Cauley TM, Williams AG (2008) Allometric 674  
 59. scaling of strength measurements to body size. *Eur J 675  
 60. Appl Physiol* 102:739–745. 676
61. Calder III WA (1983) An allometric approach to population 677  
 62. cycles of mammals. *J. Theor. Biol.* 100:275–282. 678
63. Peterson RO, Page RE, Dodge KM (1984) Wolves, Moose, 679  
 64. and the Allometry of Population Cycles. *Science* 224:1350– 680  
 65. 1352. 681
66. Krukonis G, Schaffer WM (1991) Population cycles in mam- 682  
 67. mals and birds: Does periodicity scale with body size? *J. 683  
 68. Theor. Biol.* 148:469–493. 684
69. Hendriks AJ, Mulder C (2012) Delayed logistic and Rosen- 685  
 70. zweig–MacArthur models with allometric parameter setting 686  
 71. estimate population cycles at lower trophic levels well. *Eco- 687  
 72. logical Complexity* 9:43–54. 688
73. Kendall BE, et al. (1999) Why do populations cycle? A syn- 689  
 74. thesis of statistical and mechanistic modeling approaches. 690  
*Ecology* 80:1789–1805. 691
75. Höglstedt G, Seldal T, Breistol A (2005) Period length in 692  
 76. cyclic animal populations. *Ecology* 86:373–378. 693
77. Kendall, Prendergast, Bjornstad (1998) The macroecology 694  
 78. of population dynamics: taxonomic and biogeographic pat- 695  
 79. terns in population cycles. *Ecol. Lett.* 1:160–164. 696
80. Brown J, Marquet P, Taper M (1993) Evolution of body 697  
 81. size: consequences of an energetic definition of fitness. *Am. 698  
 82. Nat.* 142:573–584. 699
83. West GB, Brown JH, Enquist BJ (1997) A General Model 700  
 84. for the Origin of Allometric Scaling Laws in Biology. *Sci- 701  
 85. ence* 276:122–126. 702
86. West GB, Woodruff WH, Brown JH (2002) Allometric scal- 703  
 87. ing of metabolic rate from molecules and mitochondria to 704  
 88. cells and mammals. *Proc. Natl. Acad. Sci. USA* 99:2473– 705  
 89. 2478. 706
90. Millar J, Hickling G (1990) Fasting Endurance and the 707  
 91. Evolution of Mammalian Body Size. *Funct. Ecol.* 4:5–12. 708
92. Alroy J (1998) Cope's rule and the dynamics of body 709  
 93. mass evolution in North American fossil mammals. *Science* 710

- 718 280:731.
- 719 60. Clauset A, Redner S (2009) Evolutionary Model of Species 738  
720 Body Mass Diversification. *Phys. Rev. Lett.* 102:038103. 739
- 721 61. Smith FA, et al. (2010) The Evolution of Maximum Body 740  
722 Size of Terrestrial Mammals. *Science* 330:1216–1219. 741
- 723 62. Saarinen JJ, et al. (2014) Patterns of maximum body size 742  
724 evolution in Cenozoic land mammals: eco-evolutionary pro- 743  
725 cesses and abiotic forcing. *Proc Biol Sci* 281:20132049– 744  
726 20132049.
- 727 63. Damuth J (1987) Interspecific allometry of population den- 746  
728 sity in mammals and other animals: the independence of 747  
729 body mass and population energy-use. *Biological Journal 748  
of the Linnean Society* 31:193–246.
- 731 64. Allen AP, Brown JH, Gillooly JF (2002) Global Biodiver- 749  
732 sity, Biochemical Kinetics, and the Energetic-Equivalence 750  
733 Rule. *Science* 297:1545–1548.
- 734 65. Enquist BJ, Brown JH, West GB (1998) Allometric scal- 751  
735 ing of plant energetics and population density : Abstract : 752  
736 Nature. *Nature* 395:163–165.
- 737 66. Kempes CP, Wang L, Amend JP, Doyle J, Hoehler T (2016)  
738 Evolutionary tradeoffs in cellular composition across diverse  
739 bacteria. *ISME J* 10:2145–2157.
- 740 67. Tilman D (1981) Tests of Resource Competition Theory Us-  
741 ing Four Species of Lake Michigan Algae. *Ecology* 62:802–  
742 815.
- 743 68. Dutkiewicz S, Follows MJ, Bragg JG (2009) Modeling the  
744 coupling of ocean ecology and biogeochemistry. *Global Bio-  
745 geochem. Cycles* 23:1–15.
- 746 69. Barton AD, Dutkiewicz S, Flierl G, Bragg J, Follows MJ  
747 (2010) Patterns of Diversity in Marine Phytoplankton. *Sci-  
748 ence* 327:1509–1511.

749 **ACKNOWLEDGMENTS.** We thank Luis Bettencourt, Jean Philippe Gibert,  
750 Eric Libby, and Seth Newsome for helpful discussions and comments on the  
751 manuscript. J.D.Y. was supported by startup funds at the University of California,  
752 Merced, and an Omidyar Postdoctoral Fellowship at the Santa Fe Institute. C.P.K.  
753 was supported by an Omidyar Postdoctoral Fellowship at the Santa Fe Institute.  
754 S.R. was supported by grants DMR-1608211 and 1623243 from the National  
755 Science Foundation, and by the John Templeton Foundation, all at the Santa Fe  
756 Institute.

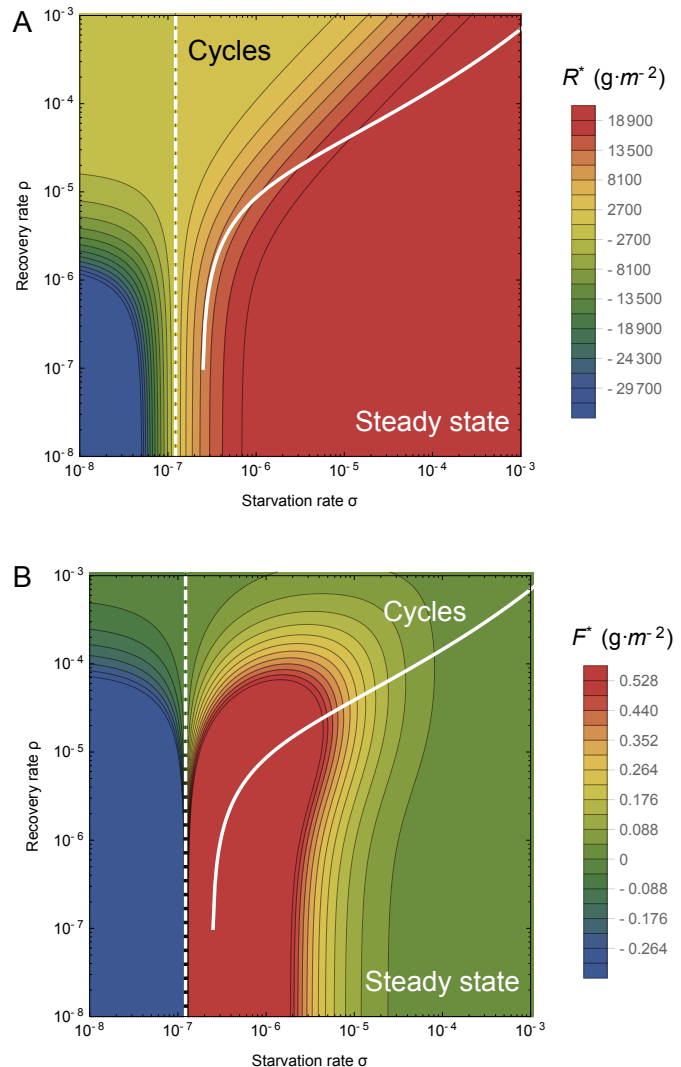


Fig. 1: The transcritical (dashed) and Hopf bifurcation (solid) as a function of the starvation rate  $\sigma$  and recovery rate  $\rho$  for a 100g consumer. These bifurcation conditions separate parameter space into unphysical, cyclic, and steady state dynamic regimes. The colors show the steady state densities for (A) the resource  $R^*$  and the (B) energetically replete consumers  $F^*$ , (warmer colors denote higher densities). Steady state densities for the energetically deficient consumers  $H^*$  (not shown) scale with those for  $F^*$ .

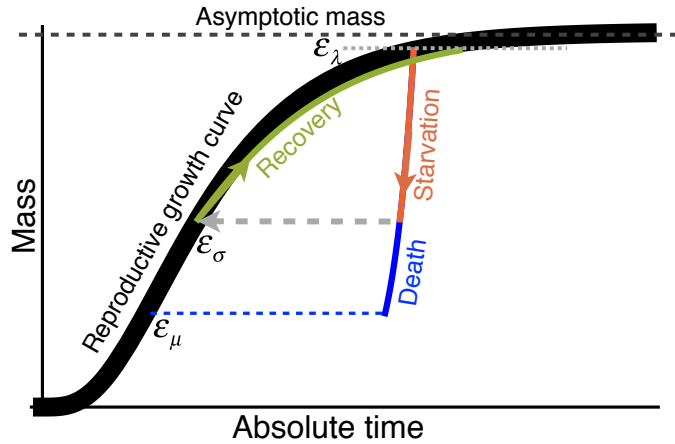


Fig. 2: The growth trajectory over absolute time of an individual organism as a function of body mass. Initial growth follows the black trajectory to an energetically replete reproductive adult mass  $m = \epsilon_\lambda M$  which we assume is 95% asymptotic mass  $M$ . Starvation follows the red trajectory to  $m = \epsilon_\sigma \epsilon_\lambda M$ . Recovery follows the green curve to the replete adult mass, where this trajectory differs from the original growth because only fat is being regrown which requires different energetics and a longer time to reach  $\epsilon_\lambda M$ . Alternatively, death from starvation follows the blue trajectory to  $m = \epsilon_\mu \epsilon_\lambda M$ .

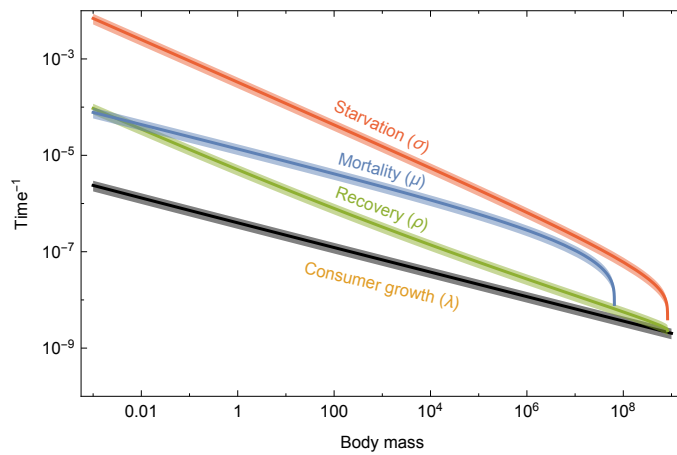


Fig. 3: Allometrically constrained starvation rate  $\sigma = 1/t_\sigma$  (red), mortality  $\mu = 1/t_\mu$  (blue) and recovery rate  $\rho = 1/t_\rho$  (green) relative to the reproductive rate  $\lambda = 1/t_\lambda$  (black) as a function of body mass (see Equations 5, 6, 10, and 11). The rate of starvation is greater than the rate of reproduction for all realized terrestrial endotherm body sizes. Mean values  $\pm 25\%$  variation are shown by the shaded region for each rate.

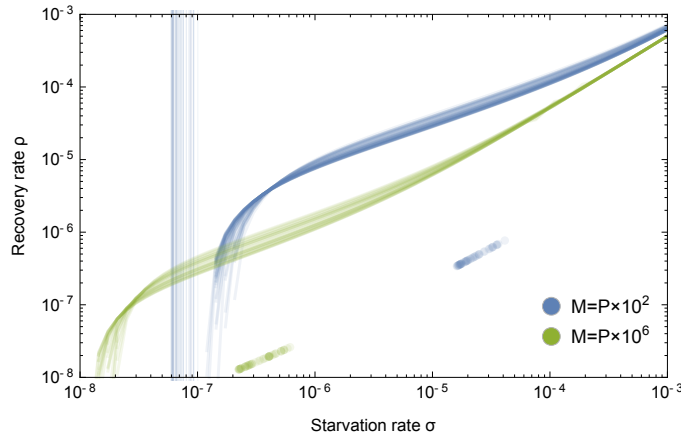


Fig. 4: Transcritical (vertical lines) and Hopf bifurcations (curves) for allometrically determined starvation  $\sigma$  and recovery  $\rho$  rates as a function of different mammalian body sizes:  $M = P \times 10^2\text{g}$  (blue) and  $M = P \times 10^6\text{g}$  (green), where  $P$  is a random uniform variable in [1, 9]. Points denote realized values of  $\sigma$  and  $\rho$  given the drawn values for  $M$ .

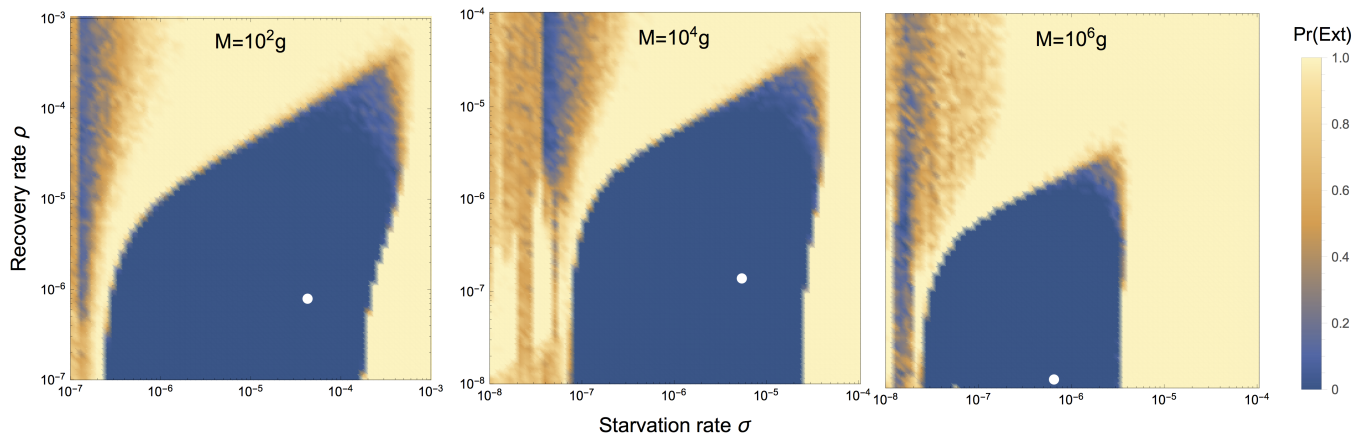


Fig. 5: Probability of extinction for a consumer with (from left to right)  $M = 10^2, 10^4, 10^6\text{g}$  as a function of the starvation rate  $\sigma$  and recovery rate  $\rho$ , where the initial density is given as  $(XF^*, XH^*, R^*)$ , where  $X$  is a random uniform variable in [0, 2]. Note the change in scale for  $M = 10^4, 10^6\text{g}$ . Extinction is defined as the population trajectory falling below  $0.2 \times$  the allometrically constrained steady state. The white points denote the allometrically constrained starvation and recovery rate.

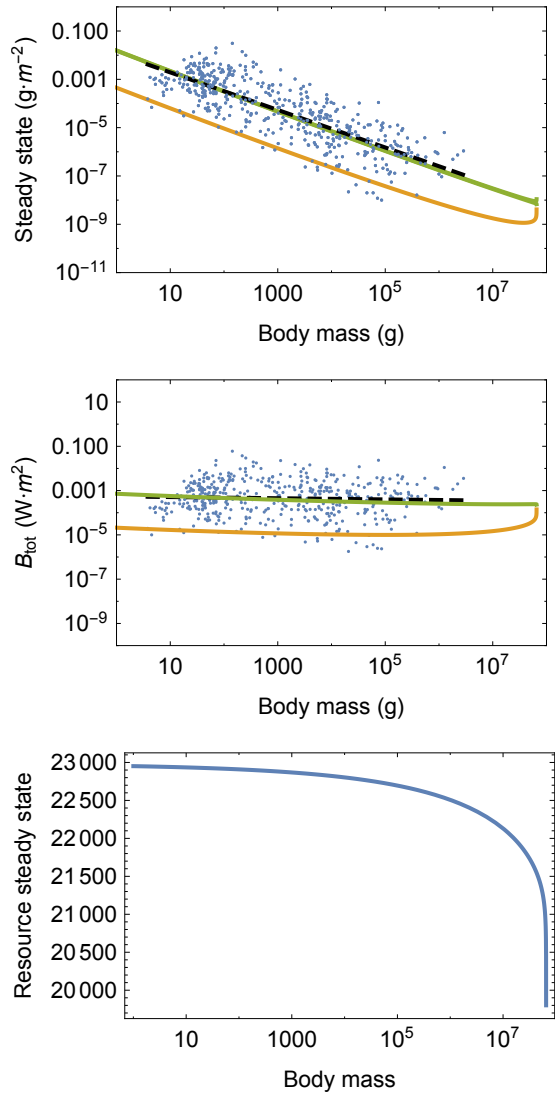


Fig. 6: (A) Consumer steady states  $F^*$  (green) and  $H^*$  (orange) as a function of body mass. (B) Total energetic use  $B_{\text{tot}}$  of consumer populations at the steady state as a function of body mass. (C) Resource steady state  $R^*$  as a function of consumer body mass. The data are from Damuth (63) and have been converted to total population metabolism using the allometric relationships for metabolic rate (please see SI and Refs. (42, 43, 45)).

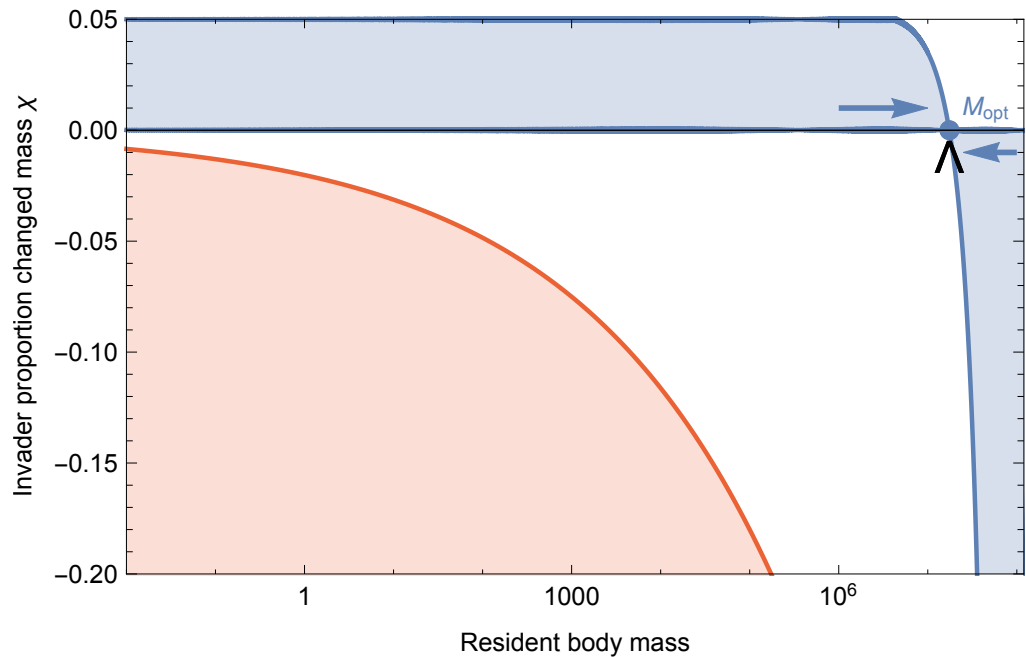


Fig. 7: Invasion feasibility for organisms with a proportional change in mass  $\chi$  against a population with a resident body mass  $M$ . The blue region denotes proportions of modified mass  $\chi$  resulting in successful invasion. The red region denotes values of  $\chi$  that result in a mass that is below the starvation threshold and is thus infeasible. Arrows point to the predicted optimal mass  $M_{\text{opt}} = 1.75 \times 10^7$ , which serves as an evolutionary attractor for body mass. The black wedge points to the largest body mass known for terrestrial mammals at  $7.74 \times 10^7 \text{ g}$  (61).